Change detection using high spatial resolution remotely sensed imagery by combining evidence theory and structural similarity

WANG Min[1, 2], **ZHANG Xingyue**[1]

1. *Key Laboratory of Virtual Geographic Environment, Nanjing Normal University, Ministry of Education, Jiangsu Nanjing* 210046, *China*;
2. *State Key Laboratory of Remote Sensing Science, Beijing Normal University, Beijing* 100875, *China*

Abstract: This paper presents an evidence theory based change detection method capable of utilizing multiple image features. With a moving window, we first get the structural similarities of both time phase image visual features and construct the basic probability assignment function (BPAF) of D-S evidence theory. We then fuse all the evidence and get the changed image areas with decision rules. Comparative work on different experimental areas, combinations of change evidence and with other methods has been carried out. It shows that our method prevents effectively the detection errors from only utilizing single feature and thus improves the detection precision. Furthermore, since the image similarity is derived from image statistical features rather than original grey, texture and gradient features, this method is robust to low calibration precision.

Key words: evidence theory, change detection, high spatial resolution image, multi-feature, structural similarity

CLC number: TP751.1 **Document code:** A

Citation format: Wang M and Zhang X Y. 2010. Change detection using high spatial resolution remotely sensed imagery by combining evidence theory and structural similarity. *Journal of Remote Sensing*. **14**(3): 558—570

1 INTRODUCTION

Remote sensing image change detection is to extract ground feature changes using two phase images of the same region by digital image processing and pattern recognition (Sing, 1989). It has many applications including environment protection, agriculture resource investigation and water conservancy construction. The ground feature changes represent as the changes of image gray value, structure, shape and texture features, and they are the main clues for change detection. Since gray values are the most feasible image feature, they are widely used in change detection. A lot of methods have been proposed including band ratio, band difference, regression model, NDVI, and PCA (Lu *et al*., 2004). Among these methods, the band difference method is the simplest, which first obtains a difference image by subtract one time phase image from the other, and distinguishes changed or unchanged pixels with some threshold. This kind of method has many shortcomings. Firstly, it is difficult to specify the threshold in many cases (Bruzzone & Prieto, 2000). Secondly, image features need to be precisely extracted from the same position of different time phase images, which puts forward rigid precision criterion to radiant calibration and image registration (Lu *et al*., 2004; Zhong & Wang, 2005).

With the rapid development of spaceflight, sensors and computer technologies, the spatial resolution of remote sensing has improved significantly. High spatial resolution remotely sensed imagery is with voluminous data, more ground details, and more serious spectral confusion. It makes traditional change detection methods only relying on image spectrum not applicable (Yuan & Song, 2007). In high spatial resolution remote sensing applications, it has already become a hot spot to develop new change detection methods based on steadier image visual features.

Compared with image gray values, edge, texture and gradient are steadier features which are less influenced by time phases. Furthermore, different visual features are comple- mented evidence for image interpretation. For example, texture is the descriptor of image gray value distribution; gradient represents the variation degree of neighborhood gray values, and edge often locates on the boundaries of spatial objects. It might cause undetection or misdetection using single feature in change detection. Based on the above reasons, many non- gray-value- based and multi-feature-based change detection methods have been proposed. For example, Fang *et al.* (2005) proposed an edge based change detection method; Liu *et al.* (2005) proposed a method based on texture or gradient similarity validation. Neil *et al.* (2001) and Zhong *et al*. (2006) implemented change detec-

Received: 2009-04-12; **Accepted**: 2009-07-04

Foundation: Chinese National Natural Science Foundation (No. 40871189), Chinese National Programs for High Technology Research and Development (No. 2007AA12Z224, No. 2009AA12Z148), and Open Fund of Laboratory for Remote Sensing Science, Beijing Normal University and the Institute of Remote Sensing Applications of Chinese Academy of Sciences.

First author biography: WANG Min (1975—), male, Associate Professor. He was graduated from Institute of Geographic Sciences and Natural Resources Research, Chinese Academy of Sciences. His major research interest includes intelligent information extraction from remotely sensed imagery, spatial data mining, and he has published nearly 30 papers. E-mail: sysj0918@126.com

tion using line features; Yuan *et al*., (2007) carried out building change detection combining image spectrum and textures; Wan *et al.* (2008) proposed a change detection method using texture and spectral correlation coefficient, etc.

In this study, we propose a novel remote sensing image change detection method comprehensively considering edge, texture and gradient changes. We calculate the structural similarity of the three features of both time phase images, create the basic probability assignment function (BPAF) of evidence theory for each feature, and implement multi-evidence fusion. With decision rules, we get the changed image areas. Comparative work on different experimental areas, combinations of changed evidence and with other methods has been carried out. It shows that our method prevents effectively the detection errors from utilizing single feature and thus improves the detection precision.

2 METHOD PRINCIPLE AND STEPS

This method involves image visual feature extraction, feature histogram statistics, structural similarity calculation of feature vectors, and multi-evidence fusion, etc. We first introduce the basic principle of evidence theory and structural similarity, and then give the method detailed steps.

2.1 D-S evidence theory

D-S evidence theory is a mathematical tool for uncertainty modeling and reasoning (Ruthven & Lalmas, 2003). It considers both the objectivity and subjectivity of evidence in probability reasoning, which is different to Bayesian theory. The probability of evidence theory is the belief to a proposition based on evidence. The theory implements induction and estimation based on multi- source information, and then gives a correct decision.

Given a non-empty set U, we call U a frame of discernment, which is composed a series of mutual exclusive and exhaustive elements. Given a proposition A in the problem domain, it belongs to 2^U. Define BPAF: m: $2^U \rightarrow [0,1]$ in 2^U, and let

$$\begin{aligned} m(\Phi) &= 0 \\ \sum_{A \subseteq U} m(A) &= 1 \end{aligned} \tag{1}$$

where $m(A)$ represents the belief exactly committed to the subset A of U. (1) If $A \subset U$, $m(A)$ denotes the determined belief to A; (2) if $A=U$, $m(A)$ denotes an uncertain assignment; (3) if $A \subseteq U$ and $m(A)>0$, A is called a focal element of m. D-S evidence theory combines different evidence with orthogonal sum. Let $m_1, m_2, \ldots, m_n$ be n BPAFs in 2^U, their orthogonal sum is denoted as

$$m = m_1 \oplus m_2 \oplus \cdots \oplus m_n \tag{2}$$

and is defined as

$$m(\phi) = 0$$
$$m(A) = \frac{\sum_{\cap A_i = A} 1 \leqslant j \leqslant n \prod m_j(A_i)}{1-k} \quad (\forall A \subset U) \tag{3}$$

where

$$k = \sum_{\cap A_i = \phi} 1 \leqslant j \leqslant n \prod m_j(A_i)$$

and k is the conflict degree of evidence. Eq. (3) is called the Dempster's combination rule.

D-S evidence theory is an effective tool for uncertainty reasoning. It has many successful applications in the fields of remote sensing, e.g., image classification, road extraction and shadow detection from multicolor airborne images (Xiao *et al*., 2006; Deng *et al*., 2007; Zhu *et al*., 2007). In this study, it is used to combine edge, texture and gradient changes for multi-feature image change detection.

2.2 Structural similarity

Structural similarity, which was first proposed by Wang *et al*.(2004), has already been used in image quality evaluation. The structural similarity of two vectors $\boldsymbol{X}$ and $\boldsymbol{Y}$ is defined as:

$$\mathrm{SSIM}(\boldsymbol{X},\boldsymbol{Y}) = [l(\boldsymbol{X},\boldsymbol{Y})]^{\alpha} \cdot [c(\boldsymbol{X},\boldsymbol{Y})]^{\beta} \cdot [s(\boldsymbol{X},\boldsymbol{Y})]^{\gamma} \tag{4}$$

where

$$l(\boldsymbol{X},\boldsymbol{Y}) = \frac{2\mu_X \mu_Y + C_1}{\mu_X^2 + \mu_Y^2 + C_2}, \quad c(\boldsymbol{X},\boldsymbol{Y}) = \frac{2\sigma_X \sigma_Y + C_2}{\sigma_X^2 \sigma_Y^2 + C_2},$$

$$s(\boldsymbol{X},\boldsymbol{Y}) = \frac{\sigma_{XY} + C_3}{\sigma_X \sigma_Y + C_3},$$

μ_X, μ_Y, σ_X, σ_Y, σ_X^2 , σ_Y^2 and σ_{XY} are the mean, standard deviation, variance and co-variance respectively, α, β and γ are the weights, and C_1, C_2 and C_3 prevent zero division. When $\alpha=\beta=\gamma=1$, $C_3= C_2/2$, Eq. (4) can be simplified as

$$\mathrm{SSIM}(\boldsymbol{X},\boldsymbol{Y}) = \frac{(2\mu_X \mu_Y + C_1)(2\sigma_{XY} + C_2)}{(\mu_X^2 + \mu_Y^2 + C_1)(\sigma_X^2 + \sigma_Y^2 + C_2)} \tag{5}$$

In our study, the BPAFs are derived from the structural similarities of image features. Generally speaking, the similarity of vector $\boldsymbol{X}$ and $\boldsymbol{Y}$ SIM($\boldsymbol{X}$,$\boldsymbol{Y}$) should satisfy these conditions: (1) Bondedness. For example, $0 \leqslant |\mathrm{SIM}(\boldsymbol{X}, \boldsymbol{Y})| \leqslant 1$. (2) Symmetry. That is SIM($\boldsymbol{X}$, $\boldsymbol{Y}$)= SIM($\boldsymbol{Y}$, $\boldsymbol{X}$); (3) Single maximum. That is SIM($\boldsymbol{X}$, $\boldsymbol{Y}$)=1 if $\boldsymbol{X}$=$\boldsymbol{Y}$. Many commonly used similarity measures defined in vector space, including Euclidian, mahalanobis and Minkowski distances, do not satisfy bondedness. Histogram intersection does not satisfy symmetry. Correlation coefficient, as a commonly used measure, does not satisfy the single-maximum condition. As illustrated in Fig. 1, the correlation coefficient of the two parallel but not very 'close' vectors reaches 1.0. Because structural similarity is derived from the mean, variance and covariance, and satisfies all the above needs, it represents similarity better than correlation coefficient. In this example, the structural similarity is only 0.64. For its advantages, structural similarity is used to measure vector similarity and create the BPAFs.

2.3 Method steps

2.3.1 Data preparation

We first implement image registration and radiant calibra-

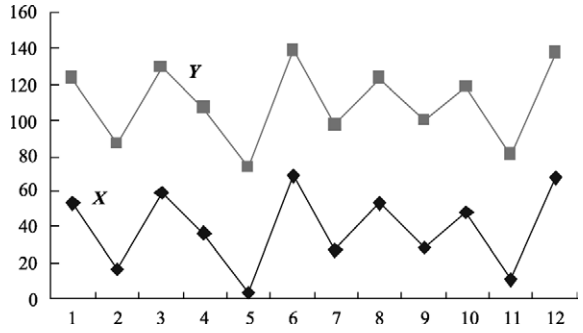

Fig. 1 Two high correlated vectors

tion for two time phase images. In our case, histogram matching is used to make pixel value distribution of an image close to the other, which causes fewer disturbances to the detection of image changes.

2.3.2 Feature extraction

We extract visual features for both time phase images. GLCM contrast is used as image texture descriptor, Canny operator to extract image edges, and Sobel operator to extract image gradient.

2.3.3 Calculation of structural similarity

With a moving window, we calculate the texture, gradient and edge similarities of the two time phase images. If the original visual features are used for similarity calculation, they are sensitive to the precision of image registration and noise. We thus construct derivate features with histogram statistics. Firstly, we quantize the gradient and texture features with Eq. (6):

$$h = \frac{x - \min}{M}$$
$$M = \frac{\max - \min}{L} \tag{6}$$

where x is the original feature value, "max" and "min" are the maximum and minimum values in this moving window respectively, and L is the quantitative level. We then create the two time phase feature histograms and calculate their structural similarities S_1 and S_2 with Eq. (5). Since edges are binary formatted, we design the edge pattern distribution histogram (EPDH) to calculate the edge similarity. EPDH is a statistical relationship descriptor of edge distribution patterns and their occurrence frequency. As illustrated in Fig. 2, in a 2×2 sub-window, there are totally 14 edge distribution patterns. Traveling the edge map with these templates and count their matching times, we get an EPDH. For example, Fig. 3(a) is the edge map in a 9×9 window, and Fig. 3(b) is the corresponding EPDH. We can then get the edge structural similarity S_3 with Eq. (5).

2.3.4 Evidence fusion and changed area extraction

We design the discernment frame $U=\{Y,N\}$, where Y represents the changed classes, and N the unchanged classes. The non-empty subsets of 2^U are $\{Y\}$, $\{N\}$, $\{Y,N\}$. Create the BPAFs according to the structural similarities of texture, gradient and

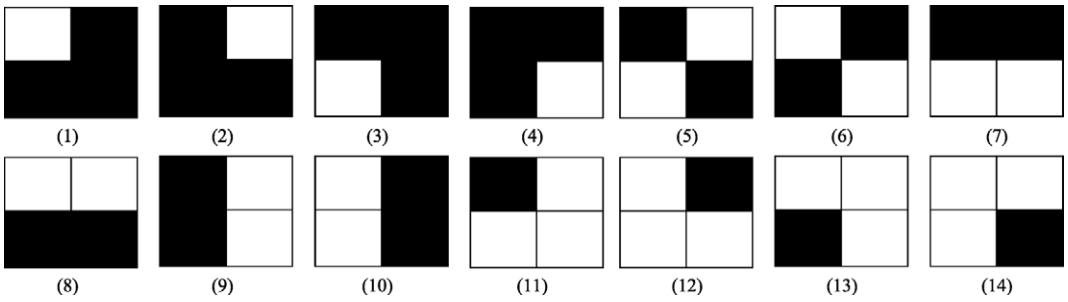

Fig. 2 Edge distribution patterns

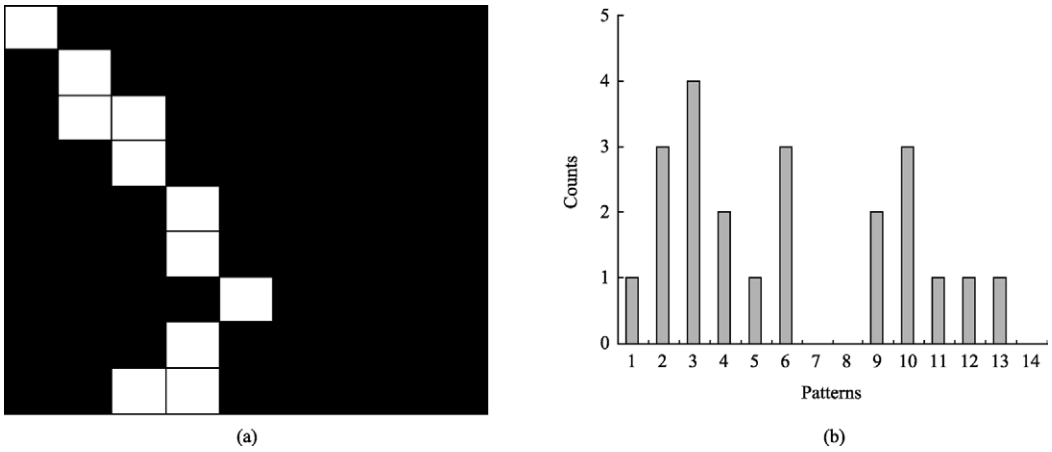

Fig. 3 Edge map and its distribution pattern histogram
(a) Edge map; (b) Distribution pattern histogram

edge with Eq. (7):

$$\begin{aligned} m_i(\{Y\}) &= (1.0 - S_i) \times \alpha_i \\ m_i(\{N\}) &= S_i \times \alpha_i \\ m_i(\{Y, N\}) &= 1.0 - \alpha_i,\ i = 1,2,3 \end{aligned} \tag{7}$$

where α_i is the trust degree of evidence to the discernment frame. Finally, we implement evidence fusion with Eq. (3). Setting suitable BPAF thresholds for changed and unchanged classes, we can then get the changed image areas.

3 EXPERIMENTAL ANALYSES

Our experimental data are ALOS imagery received in November, 2003 and December 2005 respectively, located in Jiangning, Nanjing, with spatial resolution 2.5m. As illustrated in Fig. 5(a) and Fig. 5(b), the first experimental area ranges from 31°39′49.84″N —31°40′30.01″N, 119°2′9.66″E—119°3′44.74″E, with 1012×477 pixels in size. The second experimental area ranges from 31°52′45.40″N—31°54′4.47″N, 118°46′2.58″E—118°47′35.97″E, with 999×963 pixels in size.

In the fist experimental area, we wanted to find the best evidence fusion way by comparing the seven combinations of the evidence of gradient, edge and texture. We also wanted to validate evidence theory. The second experimental area was used to verify our conclusion from experimental area 1. We thus used uniform algorithm inputs in both cases. It was as follows: the moving window size was 9×9, gray level 32, window size 5×5, orientation 0°, and inter-pixel distance 1 pixel to calculate GLCM contrast; the standard variance was 0.6, ratio of low to high threshold 0.7, and ratio of pixels with values lower than high threshold was 80%. The quantitative level was 14 to quantize texture and gradient features; C_1 and C_2 were 0.3 and 0.6 to calculate structural similarity; α_1, α_2 and α_3 were 0.9, 0.9 and 0.95 respectively for evidence fusion; the BPAF supporting image changes was larger than 0.25, or that supporting un-changes was less than 0.7.

3.1 Experiment 1

After image registration and radiant calibration, we tested the seven combination modes of evidence. Fig. 4(c) to Fig. 4(i) are the detection results; Fig. 4(j) is the detection result of similarity validation using gradient feature with similarity threshold 0.7, and Fig. 4(k) illustrates the result by combining

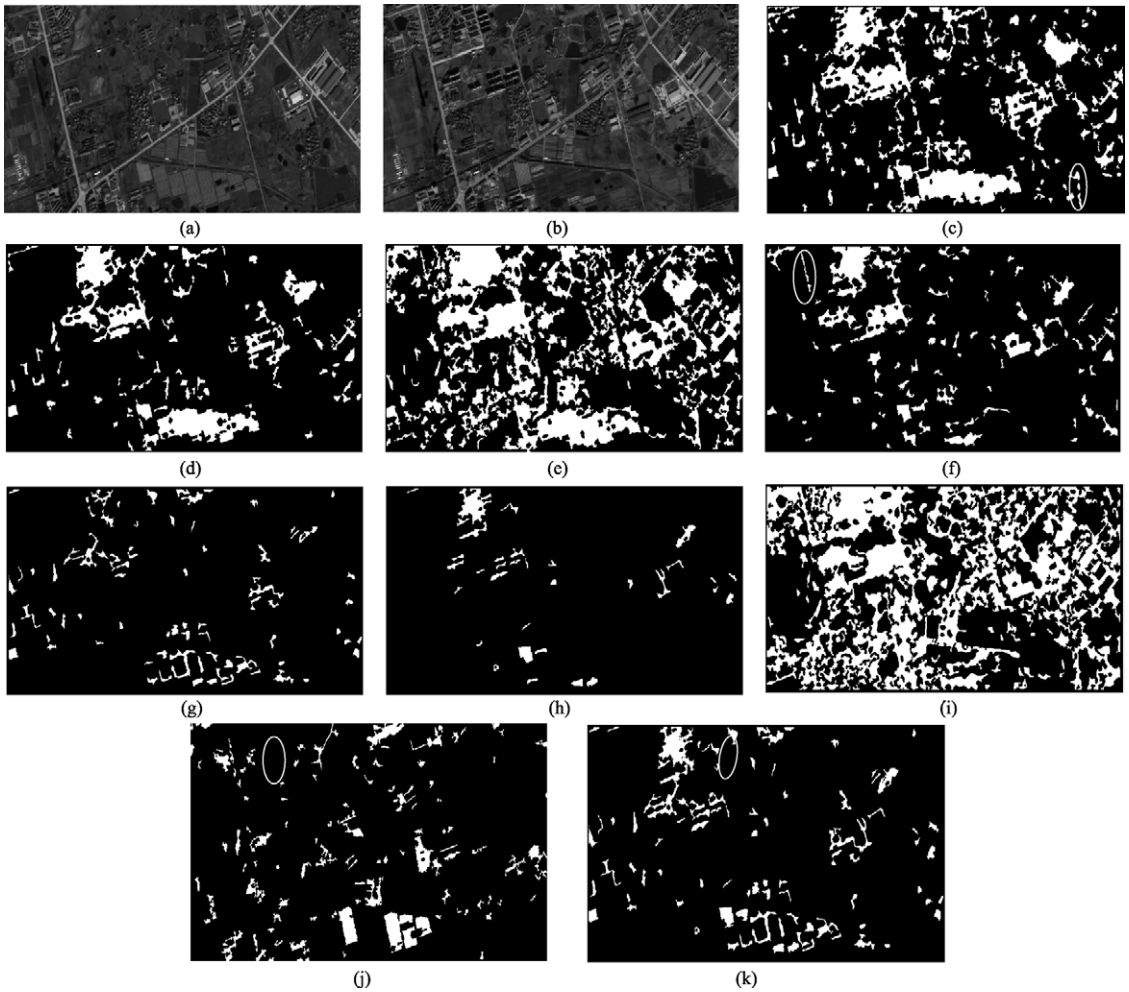

Fig. 4 First experimental area

(a) ALOS image in 2003; (b) ALOS image in 2005; (c) Fusion of gradient, texture and edge; (d) Fusion of edge and gradient; (e) Fusion of texture and edge; (f) Fusion of texture and gradient; (g) Detection with edge; (h) Detection with gradient; (i) Detection with texture; (j) Detection with similarity calibration; (k) Output of implementing 'OR' operation

edge and gradient with operator ‘OR’.

From Fig. 4(c) and Fig. 4(d), it was found that the fusion of gradient, texture and edge, or fusion of edge and gradient issued better detection, with most changed areas found. But they were with different sensitivity to changes. For example, the three-feature-fusion method recognized the bottom right area in Fig. 4(c) as a changed area which is with very tiny changes but the two-feature-fusion method omitted it.

From Fig. 4(e) to Fig. 4(i), we found that the fusion of texture and edge is very sensitive to changes, which detected most changed areas but with a lot of misdetection. Fusion of texture and gradient, which is not very sensitive to changes, detected a lot of changed areas but with un-detection and a lot of misdetection (see an example in Fig. 4(f)). Single feature detection using edge or gradient issued serious un-detection results. On the contrary, the method using single texture was with serious misdetection. As illustrated in Fig. 4(j), similarity validation method detected many changed areas but with serious misdetection.

We combined the detection results using edge and gradient features by operation ‘OR’, and compared it with that of the fusion of edge and gradient method. As exemplified in the marked changed area in Fig. 4(k), the former was with serious un-detection results, while the two-feature fusion method issued correct detection. It proves that evidence theory is an effective method for uncertainty induction, not simple pileup of multi-evidence.

3.2 Experiment 2

We used the same algorithm inputs in experimental area 2. Fig. 5(c) and Fig. 5(d) are the detection of fusing gradient, texture and edge, and of fusing edge and gradient. We got fairly results without any tuning of inputs. In this area, the three-feature-fusion

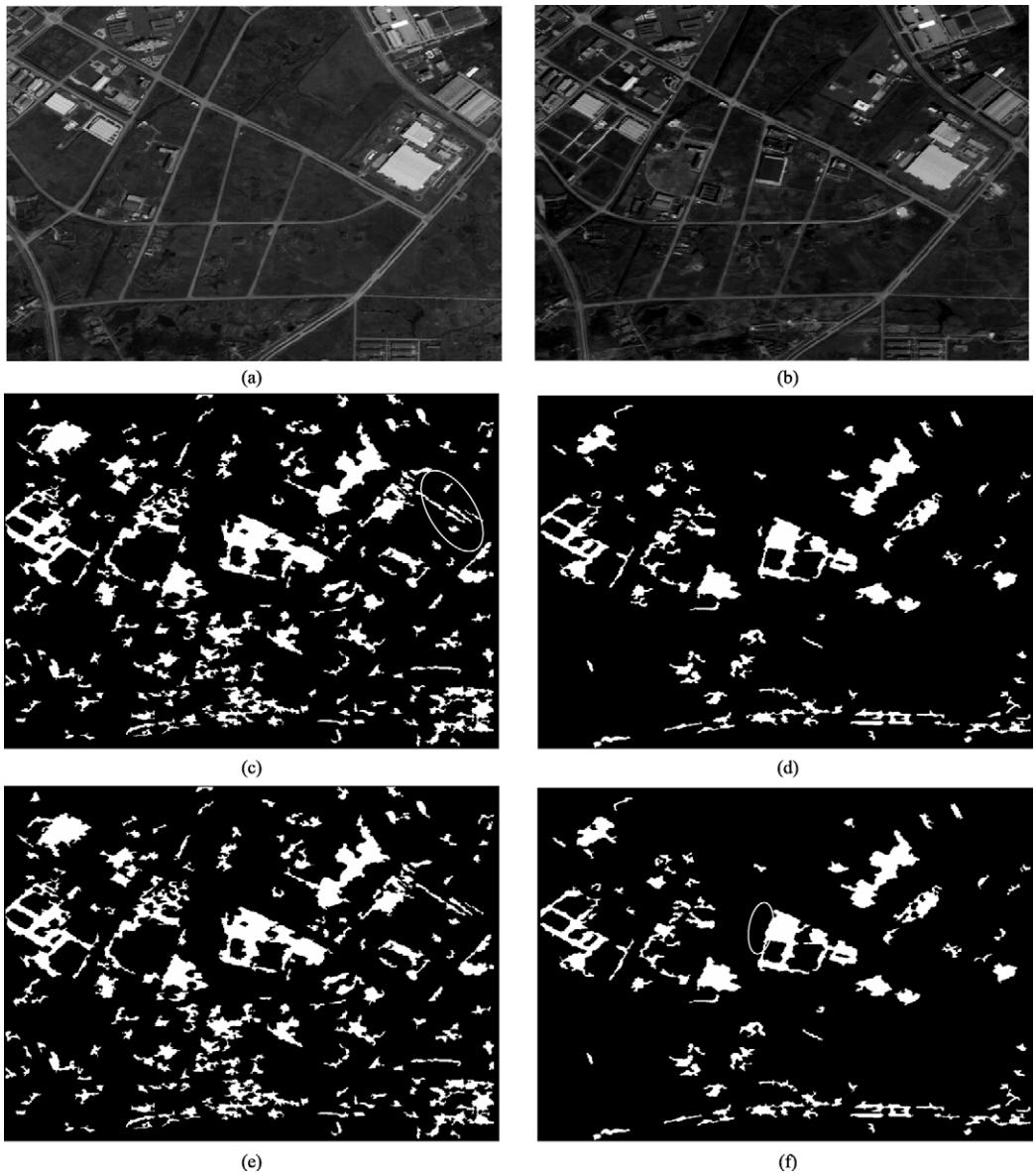

Fig. 5 Second experimental area

(a) ALOS image in 2003; (b) ALOS image in 2005; (c) Fusion of gradient, texture and edge; (d) Fusion of edge and gradient; (e) Three features without radiant calibration; (f) Two features without calibration

method was more sensitive to image detailed changes, which brought some misdetection, while the two-feature-fusion method detected most changed areas but overlooked some detailed changes.

To investigate the influence of preprocessing to the detection, we carried out detection only with image calibration and left out radiant calibration. The results are illustrated in Fig. 5(e) and Fig. 5(f). Comparing them with Fig. 5(c) and Fig. 5(d), we found the differences were very small (see Fig. 5(f)). It shows that our method is robust to the precision of radiant calibration, since the steadier statistical features, not the original image visual features are utilized in change detection.

We got the actual changed areas by visual interpretation, overlaid it with the auto detection results, and then got the precision statistics in the two experimental areas (see Table 1). We found that the total detection precision in area 2 declines slightly, which verifies that our method is robust to the algorithm inputs. Furthermore, the three-feature and two-feature-fusion methods show little difference in total detection precision, while the former issued 10%—15% false alarm. It is because texture is involved in the three-feature-fusion detection, which makes it more sensitive to detailed changes.

Table 1 Detection precision

Experimental area	Method	Total accuracy /%	Changed pixels	Changed pixels detected and correct detection ratio		Unchanged pixels detected and false alarm ratio	
Experimental area 1	Similarity validation method	43.6	55093	25015	45.4%	1012	1.8%
	Fusion of edge and gradient	81.5		50057	90.8%	5178	9.3%
	Fusion of gradient, texture and edge	82.8		51239	93.0%	5627	10.2%
	Fusion of texture and edge	77.9		53189	96.5%	10293	18.6%
	Fusion of texture and gradient	74.7		45698	82.9%	4527	8.2%
	Edge	33.8		19085	34.6%	454	0.8%
	Gradient	33.8		18954	34.4%	341	0.6%
	Texture	66.7		55093	100%	18362	33.3%
Experimental area 2	Similarity validation method	47.1	116839	56324	48.2%	1354	1.1%
	Fusion of edge and gradient	75.4		89547	76.6%	1495	1.2%
	Fusion of gradient, texture and edge	79.1		109153	93.4%	16784	14.3%
	Fusion of texture and edge	59.0		90312	77.2%	21293	18.2%
	Fusion of texture and gradient	57.4		81564	69.8%	14527	12.4%
	Edge	25.8		34121	29.2%	4054	3.4%
	Gradient	30.0		38659	33.1%	3601	3.1%
	Texture	68.1		116839	100%	37362	31.9%

4 CONCLUSION

In this study, we propose a novel remote sensing image change detection method by fusing multi-features. We first get the structural similarities of both images and construct the BPAFs of D-S evidence theory. We then fuse all the evidence and get the changed areas. Comparative work shows that our method prevents effectively the detection errors from only utilizing single feature and thus improves the detection precision. Furthermore, since the image similarity is derived from image statistical features rather than original grey, texture and gradient features, this method is robust to low calibration precision. We also point out the openness of this method since we can easily add and combine different evidence to improve its detection precision and applicability.

REFERENCES

Bruzzone L and Prieto D F. 2000. Automatic analysis of the difference image for unsupervised change detection. *IEEE Transactions on Geoscience and Remote Sensing*, **38**(3): 1171—1182

Deng W, Shao X, Liu H, Wan G and Xu L. 2007. Discussion of remote sensing image classification method based on evidence theory. *Journal of Remote Sensing*, **11**(4): 568—573

Fang S, Dian Y and Li W. 2005. Change detection based on both edges and gray. *Geomatics and Information Science of Wuhan University*, **30**(2): 135—138

Liu Z, Gong P, Shi P, Sasagawa T and He C. 2005. Study on change detection automatically based on similarity calibration. *Journal of Remote Sensing*, **9**(5): 537—543

Lu D, Mausel P, Brondízio E and Moran E. 2004. Change detection techniques. *International Journal of Remote Sensing*, **25**(12): 2365—2401

Neil C R and Grewe L L. 2001. Change detection for linear features in aerial photographs using edge-finding. *IEEE Transaction on Geoscience and Remote Sensing*, **39**(7): 1608—1612

Ruthven I and Lalmas M. 2003. Using dempster-shafer's theory of evidence to combine aspects of information use. *Journal of Intelligent Information Systems*, **19**(3): 267—301

Sing A. 1989. Change detection techniques using remotely sensed data. *International Journal of Remote Sensing*, **10**(6): 989— 1003

Wan Y, Shen S and Zhang G. 2008. Change detection of multi-time remote sensing images based on statistics models. *Geomatics and Information Science of Wuhan University*, **33**(7): 669—672,710

Wang Z, Lu L, Bovik A C. 2004. Video quality assessment based on structural distortion measurement. *Signal Processing: Image Communication*, **19**(2): 121—132

Xiao Z, Bao G and Huang J. 2006. Update of road network in GIS by fusing SAR and TM imagery. *Acta Geodaetica et Cartographica Sinica*, **35**(1): 46—51

Yuan X and Song Y. 2007. A building change detection method considering projection influence Based on spectral feature and texture feature. *Geomatics and Information Science of Wuhan University*, **32**(6): 489—493

Zhong J and Wang R. 2005. Multitemporal remote sensing image change detection based on adaptive parameter estimation. *Acta Geodaetica et Cartographica Sinica*, **34**(4): 331—336

Zhong J and Wang R. 2006. Multitemporal remote sensing images change detection based on linear feature. *Journal of National University of Defense Technology*, **28**(5): 80—83

Zhu Q, Xu S and Han L. 2007. A new shadow extraction method from color aerial images based on dempster-shafer evidence theory. *Acta Automatica Sinica*, **33**(6): 588—595

多特征证据融合的遥感图像变化检测

汪 闽[1,2], 张星月[1]

1.南京师范大学 虚拟地理环境教育部重点实验室, 江苏 南京 210046;
2. 北京师范大学 遥感科学国家重点实验室, 北京 100875

摘 要: 提出了一种以证据理论综合利用图像多种特征的变化检测方法。方法利用滑动窗口计算两时相图像 3 种特征的结构相似度, 以之构建 D-S 证据理论的基本概率赋值函数并进行证据合成, 通过规则判定得到图像变化区域。通过对不同试验区、不同证据组合方式以及方法间的比较实验表明, 相对单一特征检测方法有效地提高了检测的精度。此外, 由于采用统计而非原始图像特征度量特征相似性, 方法具有对辐射、几何配准精度要求较低等优点。

关键词: 证据理论, 变化检测, 高空间分辨率遥感, 多特征, 结构相似性

中图分类号: TP751.1 文献标识码: A

引用格式: 汪 闽, 张星月. 2010. 多特征证据融合的遥感图像变化检测. 遥感学报, **14**(3): 558—570
Wang M and Zhang X Y. 2010. Change detection using high spatial resolution remotely sensed imagery by combining evidence theory and structural similarity. *Journal of Remote Sensing*. **14**(3): 558—570

1 引 言

遥感图像变化检测是利用对同一地区在不同时期拍摄的两幅或多幅遥感图像, 采用图像处理和模式识别等手段, 检测出该地区的地物变化信息的过程(Sing, 1989), 它在环境、农业、水利等诸多领域有着非常广泛的应用。地物变化在遥感图像上反映为图像灰度(光谱)、结构、形状和纹理等特征的变化, 它们同时是遥感图像变化检测的主要依据。由于图像灰度特征容易使用, 为此相关方法较多, 其中包括比值法、差值法、回归、植被指数法、主成分分析等(Lu 等, 2004) 。其中, 最简单常见的方法是利用图像差分技术得到差异图像, 利用阈值区分变化、未变化像元。此类方法阈值确定是个难题 (Bruzzone & Prieto, 2000), 且由于是两时相图像相同位置像元的特征计算, 为此对图像辐射、几何配准、校正精度要求很高(Lu 等, 2004; 钟家强&王润生, 2005)。

近年来, 随着航天技术、传感器技术、计算机技术及其相关学科的迅猛发展, 遥感技术得到了飞速发展, 遥感图像的分辨力得到极大的提高, 如 GeoEye-1 图像的空间分辨率已达到 0.41m。高空间分辨率遥感所具有的数据量庞大、地物细节明显、光谱混淆现象严重的特点造成单纯依据图像灰度特征的变化检测方法变得不太适用(袁修孝&宋妍, 2007)。为此, 依据更为稳定的图像特征、发展适合于高分辨率遥感图像的变化检测方法, 逐渐成为遥感应用的研究热点。

相对于灰度特征, 图像边缘、纹理、梯度等特征更为稳定, 不易受遥感图像时相变化的影响。此外, 不同的视觉特征是反映图像不同侧面并互为补充的图像表征, 如纹理描述了图像灰度分布的空间结构, 梯度反映了区域内相邻像元的灰度变化程度, 边缘代表了目标边界。在变化检测时, 单独使用某一特征进行变化检测有可能造成漏检或误检。基于以上原因, 目前已有许多利用其他特征乃至多特征实现变化检测的方法。例如: 方胜辉等(2005)提出了一种基于边缘特征的变化检测方法; 刘臻等(2005)提出基于相似度验证的变化检测方法, 利用梯度、纹理相似度提取变化区域; Neil 等(2001)、钟家强等(2006)采用线特征进行变化检测; 袁修孝等(2007)提出综合应用光谱和纹理特征对建筑物进行变化检测; 万幼川等(2008)提出应用纹理和光谱相关系数进行

收稿日期: 2009-04-12; 修订日期: 2009-07-04

基金项目: 国家自然科学基金(编号: 40871189), 国家 863 课题(编号: 2007AA12Z224, 编号: 2009AA12Z148)和遥感科学国家重点实验室(北师大)开放基金。

第一作者简介: 汪 闽(1975—), 男, 南京师范大学副教授, 博士, 主要研究方向为遥感图像处理与信息提取, 空间数据挖掘。以第一作者发表论文近 30 篇。E-mail: sysj0918@126.com。

变化检测等。

本文提出一种新的融合多特征的遥感图像变化检测方法。该方法将图像的边缘分布变化、纹理特征变化和梯度特征变化看作是变化检测的多个证据源，通过计算两时相图像的多种特征的结构相似度构建 D-S 证据理论的基本概率赋值函数 (basic probability assignment function, BPAF)并进行证据合成，最后通过规则判定得到时相间区域是否变化的结论。通过对不同试验区、不同证据组合方式以及方法间的比较实验表明，该方法有效避免了基于单一特征进行变化检测所造成的漏检或误检，并且对辐射、几何配准精度要求较低，为此具有较强的应用价值。

2　原理与步骤

该方法主要涉及图像视觉特征提取、特征直方图统计构建特征向量、特征向量的结构相似度计算以及基于多特征的证据融合等环节。

2.1　D-S 证据理论

D-S 证据理论(Ruthven & Lalmas, 2003)作为一种数学工具，它允许人们对不精确、不确定性问题进行建模，并进行推理，这为不确定信息的处理提供了新的思路。与贝叶斯理论不同，它认为对于概率推断的理解，不仅要强调证据的客观性，也要强调证据的主观性。概率是人们在证据的基础上构造出的对一命题的信任程度，D-S 证据理论可以根据各源信息对系统整体进行归纳和估计，做出正确的决策。

对于一个非空集合 U，称 U 为辨别框架，它由一系列互斥且穷举的元素组成。对于问题域中任意命题 A，都应属于幂集 2^U。在 2^U 上定义 BPAF: m: $2^U\rightarrow[0,1]$，使 m 满足

$$\begin{aligned} m(\Phi)&=0\\ \sum_{A\subseteq U} m(A)&=1 \end{aligned} \tag{1}$$

式中，$m(A)$表示证据对 U 的子集 A 的一种信任度量。$m(A)$的意义如下: (1) 若 $A\subset U$，则 $m(A)$表示对 A 的确定信任度; (2) 若 $A=U$，则 $m(A)$表示这个数不知如何分配; (3) 若 $A\subseteq U$，且 $m(A)>0$，则称 A 是 m 的一个焦元。D-S 证据理论采用正交和组合不同的证据源。设 m_1, m_2, …, m_n 为 2^U 上的 n 个 BPAF，它们的正交和表示为:

$$m=m_1\oplus m_2\oplus\ldots\oplus m_n \tag{2}$$

且定义为

$$m(\phi)=0$$

$$m(A)=\frac{\sum\limits_{\cap A_i=A}\prod\limits_{1\leqslant j\leqslant n} m_j(A_i)}{1-k}\ (\forall A\subset U) \tag{3}$$

其中

$$k=\sum_{\cap A_i=\phi}\prod_{1\leqslant j\leqslant n} m_j(A_i)$$

式中，k 反映了证据的冲突程度。公式(3)也称为 Dempster 合成法则。

D-S 证据理论是解决不确定性推理问题的有效工具。目前在遥感图像处理与信息提取领域，已有许多成功应用案例，其中包括遥感图像分类(邓文胜等，2007)、道路提取(肖志强等，2006)、彩色航空影像阴影检测(朱庆等, 2007)等。本文利用它组合边缘、纹理、梯度变化特征实现变化检测。

2.2　结构相似度

Wang 等(2004)最早提出了结构相似度(structural similarity)的概念并将其应用于图像质量评价。向量 $\boldsymbol{X}$ 与 $\boldsymbol{Y}$ 的结构相似度定义为:

$$\begin{aligned} \mathrm{SSIM}(\boldsymbol{X},\boldsymbol{Y})=&[l(\boldsymbol{X},\boldsymbol{Y})]^{\alpha}\cdot\\ &[c(\boldsymbol{X},\boldsymbol{Y})]^{\beta}\cdot[s(\boldsymbol{X},\boldsymbol{Y})]^{\gamma} \end{aligned} \tag{4}$$

其中:

$$l(\boldsymbol{X},\boldsymbol{Y})=\frac{2\mu_X\mu_Y+C_1}{\mu_X^2+\mu_Y^2+C_2},\quad c(\boldsymbol{X},\boldsymbol{Y})=\frac{2\sigma_X\sigma_Y+C_2}{\sigma_X^2\sigma_Y^2+C_2},$$

$$s(\boldsymbol{X},\boldsymbol{Y})=\frac{\sigma_{XY}+C_3}{\sigma_X\sigma_Y+C_3}。$$

μ_X, μ_Y, σ_X, σ_Y, σ_X^2, σ_Y^2, σ_{XY} 分别是 $\boldsymbol{X}$ 与 $\boldsymbol{Y}$ 的均值、标准差、方差和协方差。α，β，γ 是 3 个分量的权重，C_1, C_2, C_3 是为了防止当分母接近零时产生不稳定现象所添加的常数。当 $\alpha=\beta=\gamma=1$, $C_3=C_2/2$ 时，公式(4)可以简化为:

$$\mathrm{SSIM}(\boldsymbol{X},\boldsymbol{Y})=\frac{(2\mu_X\mu_Y+C_1)(2\sigma_{XY}+C_2)}{(\mu_X^2+\mu_Y^2+C_1)(\sigma_X^2+\sigma_Y^2+C_2)} \tag{5}$$

在利用证据理论进行证据推理时，需要设计各个证据的 BPAF。本文中它们由两时相图像各特征的结构相似度派生出来。一般而言，特征向量 $\boldsymbol{X}$ 和 $\boldsymbol{Y}$ 的相似性度量 SIM($\boldsymbol{X}$, $\boldsymbol{Y}$)满足以下条件比较适宜: (1)有界: 如 $0\leqslant|\mathrm{SIM}(\boldsymbol{X},\boldsymbol{Y})|\leqslant1$，越接近于 0，表示两向量相似性越弱; 越接近于 1，表示两向量相似性越强; (2)对称: 即 SIM($\boldsymbol{X}$, $\boldsymbol{Y}$)=SIM($\boldsymbol{Y}$, $\boldsymbol{X}$); (3)唯一最大值: 即 SIM($\boldsymbol{X}$, $\boldsymbol{Y}$)=1，当且仅当 $\boldsymbol{X}=\boldsymbol{Y}$。在向量空间中定义的各种距离，例如欧式距离、马氏距离、明氏距离等，常作为相似性的度量指标，但是它们不满足有界性的条件。对于直方图相交，它不满足对称性的条件。此外，相关系数在某种程度上可以表征两变量之间

的相似性，但它不满足唯一最大值条件。如图 1，对于两个“平行”但并不“靠近”的特征向量，其相关系数很高，达到 1.0。而由于结构相似度综合考虑了两向量的均值、方差和协方差，为此能更好的表征特征向量之间的相似性。此例中，***X***，***Y*** 的结构相似度只为 0.64。由于结构相似性测度满足有界、对称、唯一的要求，非常适合于度量两特征向量的相似程度，为此本文用它来构建 D-S 证据理论的 BPAF。

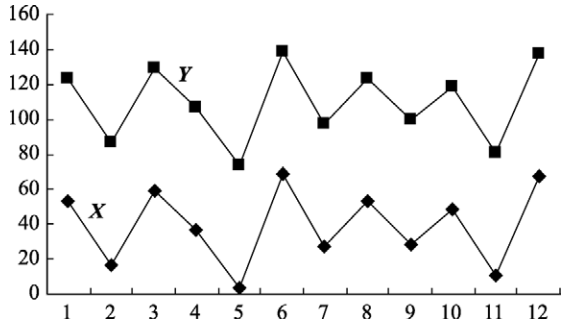

图 1 高度相关的两个向量

2.3 方法步骤

基于多特征证据融合的变化检测方法的步骤如下。

2.3.1 数据准备

选取待检测区域的两时相数据，并对数据进行必要的几何配准和相对辐射校正。如采用直方图匹配的方式，使某个时相的图像灰度值分布接近另一时相，减少不同时相的图像色调差异对变化检测带来的干扰。

2.3.2 特征提取

分别提取出两时相数据的纹理、梯度和边缘特征。其中，纹理特征选用灰度共生矩阵的对比度，边缘检测采用 Canny 算子，梯度为 Sobel 梯度。

2.3.3 结构相似度计算

在两时相遥感图像上同时开设工作窗口，进行逐行列滑动并计算两时相图像在窗口内的纹理、梯度和边缘相似度。对于纹理、梯度相似度，若直接用窗口内的原始特征值构成的特征向量进行计算，它们对图像的配准精度要求较高，且易受噪声影响。为此本文采用直方图统计的方式构建派生特征。首先对特征进行量化，量化公式为:

$$h=\frac{x-\min}{M}$$
$$M=\frac{\max-\min}{L} \tag{6}$$

其中 x 为当前要量化的值, max 和 min 分别是相应窗口中数据的最大值和最小值, L 为量化等级。将相应窗口的两时相纹理数据和梯度数据分别进行量化，统计其分布的频数，生成相应的直方图构成特征向量，然后用公式(5)计算它们之间的结构相似度 S_1 和 S_2。

边缘图像由于是二值化数据而不能沿用上述方法。为此设计了边缘模式分布直方图以计算边缘特征的结构相似度。边缘模式分布直方图描述了边缘像元分布的各种组合模式与其出现频率间的统计关系。如图 2，对于一个 2×2 的考察窗口，排列组合得到共 14 种边缘像元的分布模式。用上述 14 个模板，对两时相工作窗口内的边缘图进行遍历，记录各种模板匹配的次数，得到相应窗口的边缘模式分布直方图。例如，图 3(a)是一个 9×9 窗口的边缘数据，图 3(b)是它的模式分布直方图。据此，可同样用公式(5)计算边缘特征的结构相似度 S_3。

2.3.4 证据融合与变化区域提取

将图像的所有像元作为检测对象，定义证据理论辨别框架 U 为: $U=\{Y, N\}$。其中 Y 表示变化类, N 表示未变化类，因此 2^U 的非空子集为:$\{Y\}$，$\{N\}$，$\{Y, N\}$。然后依据两时相间工作窗口内的纹理、梯度和边缘的结构相似度构建相应的 BPAF，公式如下:

$$\begin{aligned} m_i(\{Y\})&=(1.0-S_i)\times\alpha_i \\ m_i(\{N\})&=S_i\times\alpha_i \\ m_i(\{Y,N\})&=1.0-\alpha_i,\ i=1,2,3 \end{aligned} \tag{7}$$

式中 α_i 为某证据对判别的信任度，该值依经验给出。获得以上 BPAF 后，采用公式(3)进行证据合成，对未变化类和变化类的 BPAF 分别设置适当的阈值，判断该区域是否发生变化，并将检测结果赋给窗口中心像元。对整图一次遍历后即获得变化区域。

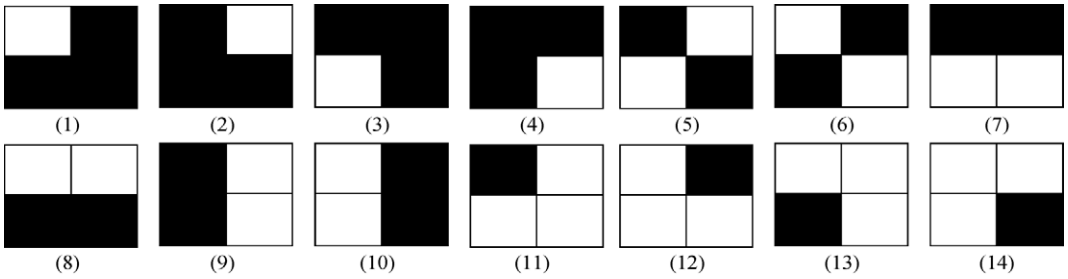

图 2 14 种边缘分布模式(黑色为背景，白色为边缘)

3　实验与分析

选用的实验数据为南京江宁区的 ALOS 全色波段数据，空间分辨率是 2.5m，成像时间分别为 2003 年 11 月和 2005 年 12 月。文中实验区一位于 31°39′49.84″N—31°40′30.01″N，119°2′9.66″E—119°3′44.74″E，图像大小为 1012×477 像元，如图 4(a)(b)所示。实验区二位于 31°52′45.40″N—31°54′4.47″N，118°46′2.58″E—118°47′35.97″E，图像大小为 999×963 像元，如图 5(a)(b)所示。

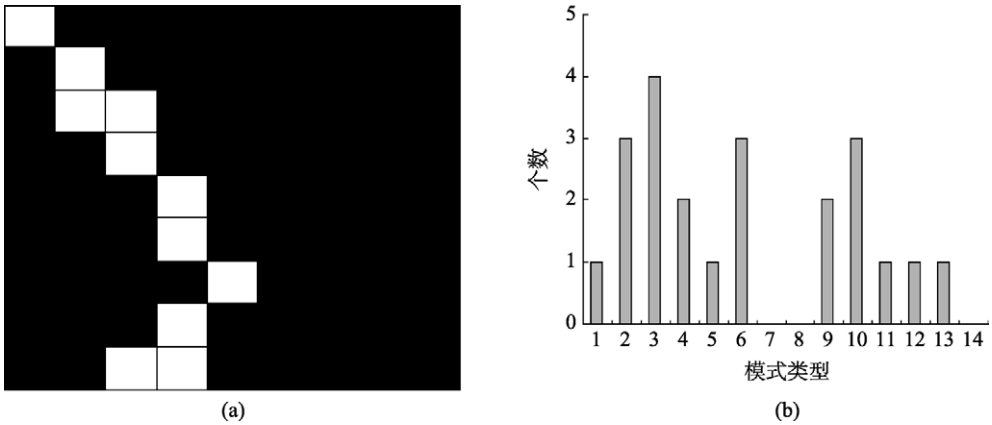

图 3　边缘图像与其模式分布直方图

(a) 边缘数据; (b) 模式分布直方图

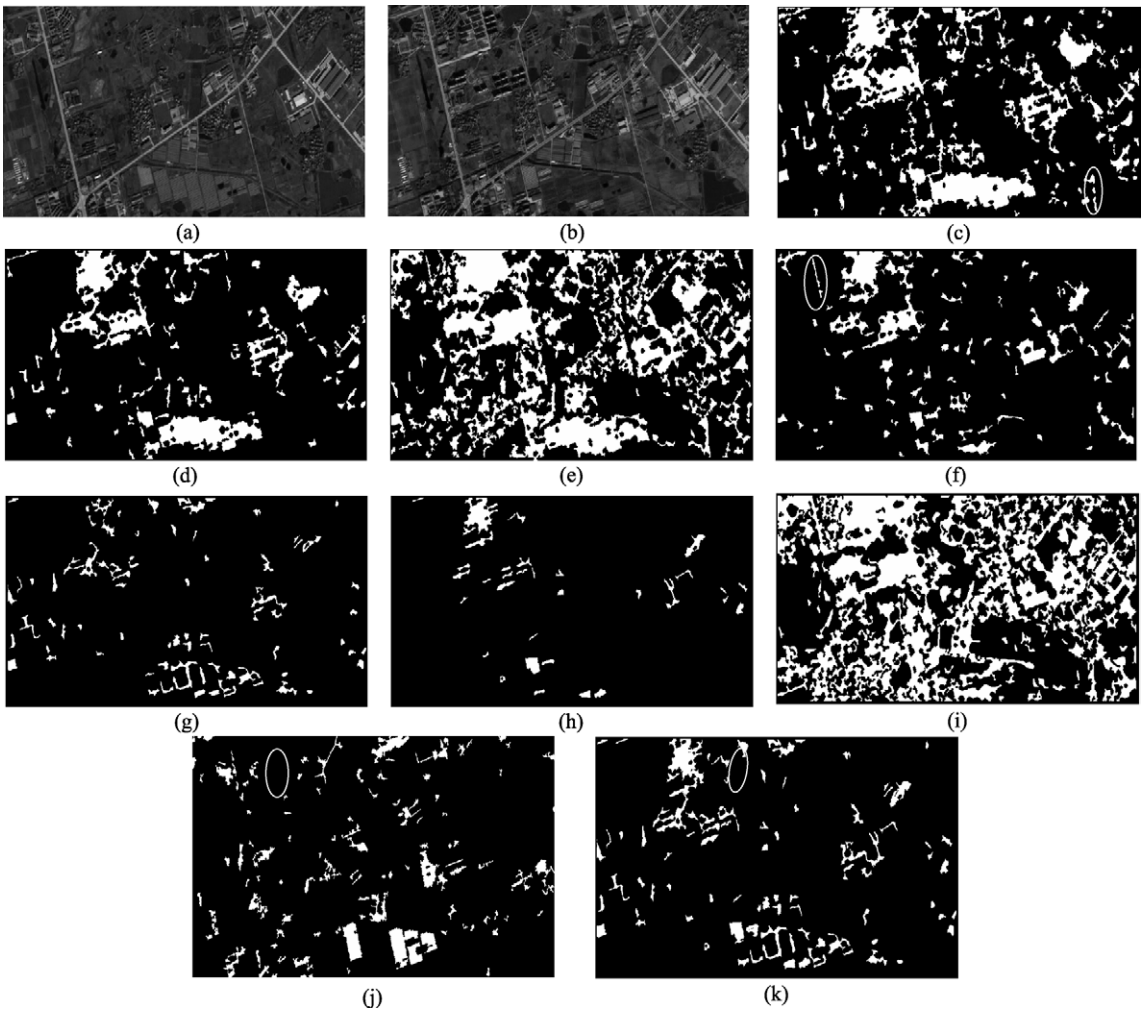

图 4　数据一及其各种检测结果

(a) 2003 年 ALOS 数据; (b) 2005 年 ALOS 数据; (c) 梯度、纹理和边缘特征融合的检测结果; (d) 边缘和梯度特征融合的检测结果; (e) 纹理和边缘特征融合的检测结果; (f) 纹理和梯度特征融合的检测结果; (g) 边缘特征的检测结果; (h) 梯度特征的检测结果; (i) 纹理特征的检测结果; (j) 基于相似度验证的检测结果; (k) 对边缘和梯度的检测结果做或运算

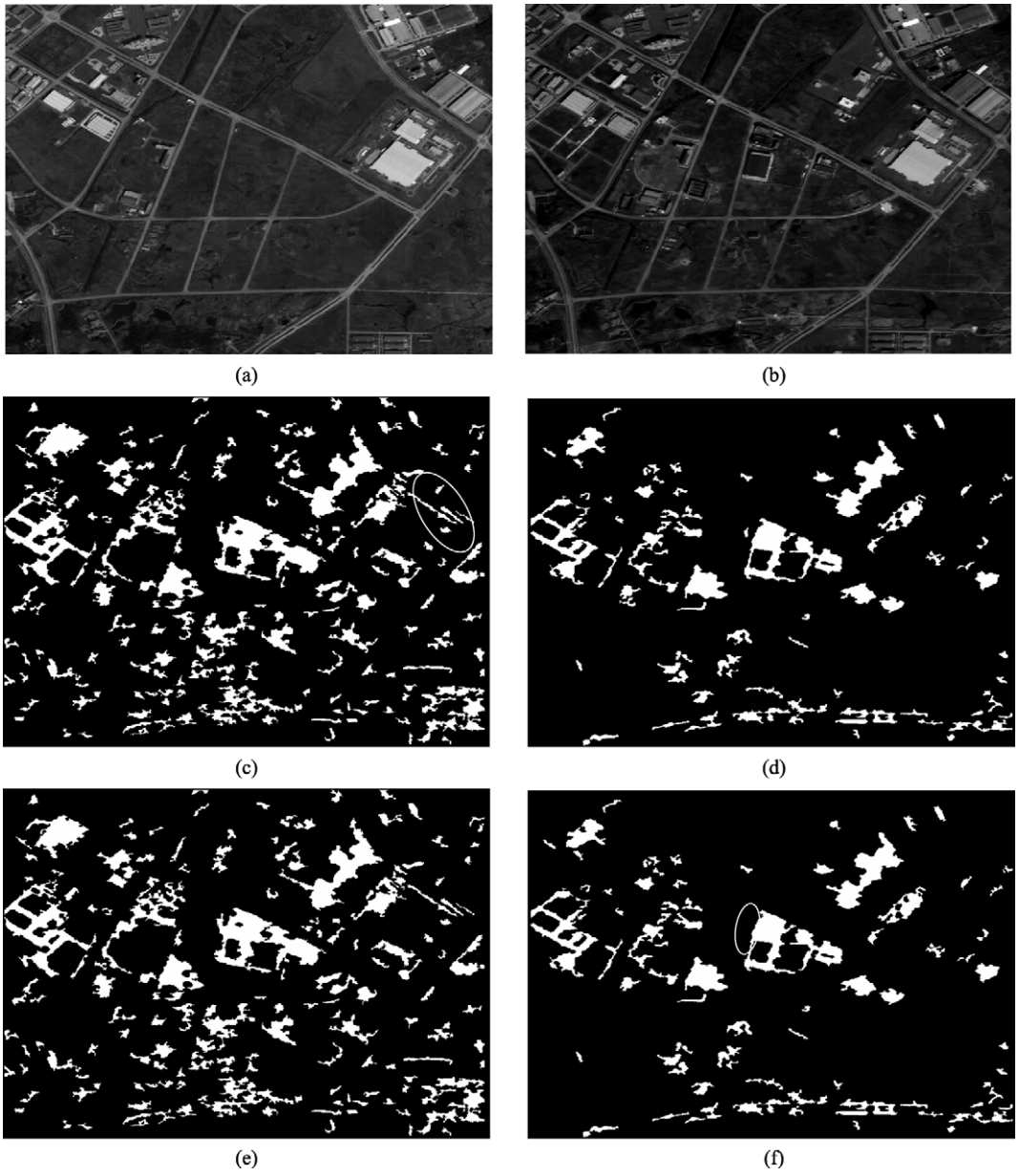

图 5 数据二及其检测结果

(a) 2003 年 ALOS 数据; (b) 2005 年 ALOS 数据; (c) 梯度、纹理和边缘特征融合的检测结果; (d) 边缘和梯度特征融合的检测结果; (e) 未辐射校正时梯度、纹理和边缘融合结果; (f) 未辐射校正时边缘和梯度融合结果

在第一个实验区，通过对梯度、边缘和纹理 3 种证据源的 7 种组合方式进行比较，寻找效果较好的组合，并对证据理论的有效性进行验证。此外，利用第二个实验区展示对有效组合方式进行推广测试的结果。基于上述目的，两个试验区所采用的算法参数完全相同。它们依次如下：滑动工作窗口大小是 9×9；计算灰度共生矩阵的对比度时，使用的灰度级数为 32，窗口为 5×5，点对间的偏离方向取 0°，偏离步长是 1 个像元。使用 Canny 算子计算两时相图像的边缘特征时，使用的标准方差为 0.6，低阈值和高阈值之比为 0.7，小于高阈值像元数占像元总数的比例为 0.8；在对纹理和梯度数据进行量化时，所采用的量化等级是 14；在计算结构相似度时，C_1 和 C_2 分别为 0.3 和 0.9；在利用证据理论进行融合时，α_1 为 0.9, α_2 为 0.9, α_3 为 0.95；在进行变化区域判定时，所采用的规则是，支持变化的 BPAF>0.25，或者支持未变化的 BPAF<0.7。

3.1 实验一

在对两时相图像进行了图像配准和相对辐射校正等预处理后，对 3 种证据源的 7 种组合方式进行了测试。图 4(c)—图 4(i)分别是各种组合方式的相应检

测结果,图 4(j)是采用梯度特征进行相似度验证的变化检测的结果(刘臻等, 2005), 经实验选取其相似度阈值为 0.7。图 4(k)是对边缘、梯度特征的检测结果进行或运算的合成结果。从图 4(c)和图 4(d)可以看出, 梯度、纹理和边缘特征三者进行融合的检测结果与边缘、梯度特征二者进行融合的检测结果好, 都能检测出主要变化区域, 但对变化的敏感度有所区别。如图 4(c)所标注的右下方区域, 仅发生了细微的变化, 3 特征融合将其检测为变化区域。从图 4(e)—图 4(i)看出, 纹理和边缘二者进行融合的方法, 对变化非常敏感, 虽然检测出了主要变化区域, 但存在一定误检。纹理和梯度特征二者进行融合的方法, 对变化相对不太敏感, 虽然检测出了一些主要变化区域, 但存在漏检, 并出现了较多误检, 如在图 4(f)所标注区域。仅仅用边缘、梯度特征进行变化检测, 漏检现象严重; 仅用纹理特征则存在大量误检。此外, 基于相似度验证的变化检测方法, 虽检测出了一些主要变化区域, 但漏检情况严重, 例如, 图 4(j)所标注的区域是一个变化区域, 但该方法未检测到。

为了测试证据理论对检测精度的贡献, 对边缘特征和梯度特征的检测结果进行或运算, 将合成结果与边缘、梯度特征证据融合的检测结果进行比较。图 4(k)是或运算结果。可以看出, 两者存在很大不同, 前者漏检现象明显。例如, 图 4(k)所标注的区域, 该区域发生了变化, 但是两特征或运算方式没有检测出来, 而两特征融合方式则检测出了变化区域。由此可见证据理论是一种有效的不确定性推理方法, 并非多证据的简单叠加。

3.2　实验二

首先对实验区二进行几何、辐射校正处理, 并采用和实验区一相同的算法参数进行实验测试。图 5(c)(d)分别是梯度、纹理和边缘三者融合与边缘、梯度特征二者融合的检测结果。注意在没有进行任何参数调节的条件下, 以上两种组合方式均取得很好的检测效果。在此区域内, 三特征融合方式对变化较敏感, 可检测出细微的变化, 同时带来部分误检, 如图 5(c)所标注的区域。两特征融合方式则检测出大多数主要变化区域而忽略了部分细节变化。

此外, 为了考察预处理精度对方法的影响, 对数据二只进行必要的几何图像配准而不做相对辐射校正, 进行变化检测, 得到图 5(e)(f)。将其与图 5(c)(d)比较, 可以发现检测结果变化非常小, 只在个别区域发生了细微的变化, 如图 5(f)所标注区域。由此可见, 该算法对辐射校正精度要求较低。其原因是由于方法是利用图像的边缘、梯度、纹理的统计特征而非直接基于图像原始特征进行变化检测, 为此参与相似性计算的特征向量比较稳定, 对辐射配准精度要求不高。

通过目视解译得到实际变化区域, 然后将各种方法的结果和其进行叠合对比得到两个实验区检测精度的统计结果(表 1)。从表 1 可以看出: (1)对于第二个试验区, 方法的总体检测精度下降不多, 说明方法对参数的依赖程度不高, 具有稳健性; (2)三特征

表 1　检测精度

实验区	变化检测方法	总检测正确率/%	变化像元数/个	检测出的变化像元数及检测率		检测出的非变化像元数及虚警率	
实验区一	相似度验证方法	43.6	55093	25015	45.4%	1012	1.8%
	边缘和梯度特征融合	81.5		50057	90.8%	5178	9.3%
	梯度、纹理和边缘特征融合	82.8		51239	93.0%	5627	10.2%
	纹理和边缘特征融合	77.9		53189	96.5%	10293	18.6%
	纹理和梯度特征融合	74.7		45698	82.9%	4527	8.2%
	边缘特征	33.8		19085	34.6%	454	0.8%
	梯度特征	33.8		18954	34.4%	341	0.6%
	纹理特征	66.7		55093	100%	18362	33.3%
实验区二	相似度验证方法	47.1	116839	56324	48.2%	1354	1.1%
	边缘和梯度特征融合	75.4		89547	76.6%	1495	1.2%
	梯度、纹理和边缘特征融合	79.1		109153	93.4%	16784	14.3%
	纹理和边缘特征融合	59.0		90312	77.2%	21293	18.2%
	纹理和梯度特征融合	57.4		81564	69.8%	14527	12.4%
	边缘特征	25.8		34121	29.2%	4054	3.4%
	梯度特征	30.0		38659	33.1%	3601	3.1%
	纹理特征	68.1		116839	100%	37362	31.9%

融合与两特征融合在总体检测精度上比较接近，其中三特征融合检测率相对较高，但同时存在 10%—15%左右的虚警。这可能是由于三特征融合方式考虑了纹理变化，会对细节变化更敏感一些，为此得到了更高的检测率。

4 结 论

本文提出了一种基于多特征证据融合的变化检测方法。该方法通过计算两时相遥感图像的多种特征的结构相似度，以之构建 D-S 证据理论的基本概率赋值函数并进行证据合成，从而实现了图像边缘、纹理、梯度等特征在变化检测中的综合使用。通过对纹理、梯度和边缘 3 种特征的 7 种不同组合方式的比较和分析，发现梯度、纹理和边缘特征三者进行融合与边缘、梯度特征两者进行融合的检测结果相对较好。由于该算法不是直接基于图像灰度或纹理、梯度等原始特征，而是基于检测窗口内的统计特征进行变化检测，算法对不同时相的图像灰度差异不敏感、对预处理的精度要求较低，具有较强的鲁棒性。应该指出，方法的技术框架是开放的，可以非常方便地加入、组合变化证据源以尝试进一步提高方法的检测精度和适用性。

REFERENCES

Bruzzone L and Prieto D F. 2000. Automatic analysis of the difference image for unsupervised change detection. *IEEE Transactions on Geoscience and Remote Sensing*, **38**(3): 1171—1182

Deng W S Shao X L, Liu H, Wan G F and Xu L. 2007. Discussion of remote sensing image classification method based on evidence theory. *Journal of Remote Sensing*, **11**(4): 568—573

Fang S, Dian Y and Li W. 2005. Change detection based on both edges and gray. *Geomatics and Information Science of Wuhan University*, **30**(2): 135—138

Liu Z, Gong P, Shi P G, Sasagawa T and He C Y. 2005. Study on change detection automatically based on similarity calibration. *Journal of Remote Sensing*, **9**(5): 537—543

Lu D, Mausel P, Brondízio E and Moran E. 2004. Change detection techniques. *International Journal of Remote Sensing*, **25**(12): 2365—2401

Neil C R and Grewe L L. 2001. Change detection for linear features in aerial photographs using edge-finding. *IEEE Transaction on Geoscience and Remote Sensing*, **39**(7): 1608—1612.

Ruthven I and Lalmas M. 2003. Using dempster-shafer's theory of evidence to combine aspects of information use. *Journal of Intelligent Information Systems*, **19**(3): 267—301

Sing A. 1989. Change detection techniques using remotely sensed data. *International Journal of Remote Sensing*, **10**(6): 989— 1003

Wan Y, Shen S and Zhang G. 2008. Change detection of multi-time remote sensing images based on statistics models. *Geomatics and Information Science of Wuhan University*, **33**(7): 669—672,710

Wang Z, Lu L, Bovik A C. 2004. Video quality assessment based on structural distortion measurement. *Signal Processing: Image Communication*, **19**(2): 121—132

Xiao Z Q, Bao G S and Huang J X. 2006. Update of road network in GIS by fusing SAR and TM imagery. *Acta Geodaetica et Cartographica Sinica*, **35**(1): 46—51

Yuan X X and Song Y. 2007. A building change detection method considering projection influence Based on spectral feature and texture feature. *Geomatics and Information Science of Wuhan University*, **32**(6): 489—493

Zhong J Q and Wang R S. 2005. Multitemporal remote sensing image change detection based on adaptive parameter estimation. *Acta Geodaetica et Cartographica Sinica*, **34**(4): 331—336

Zhong J Q and Wang R S. 2006. Multitemporal remote sensing images change detection based on linear feature. *Journal of National University of Defense Technology*, **28**(5): 80—83

Zhu Q, Xu S H and Han L T. 2007. A new shadow extraction method from color aerial images based on dempster-shafer evidence theory. *Acta Automatica Sinica*, **33**(6): 588—595

附中文参考文献

邓文胜，邵晓莉，刘海，万诰方，许亮. 2007. 基于证据理论的遥感图像分类方法探讨. 遥感学报, **11**(4): 568—573

方圣辉，佃袁勇，李微. 2005. 基于边缘特征的变化检测方法研究. 武汉大学学报. 信息科学版, **30**(2): 135—138

刘臻，宫鹏，史培军，Sasagawa T，何春阳. 2005. 基于相似度验证的自动变化探测研究. 遥感学报, **9**(5): 537—543

万幼川，申邵洪，张景雄. 2008. 基于概率统计模型的遥感影像变化检测. 武汉大学学报. 信息科学版，**33**(7): 669—672, 710

肖志强，鲍光淑，黄继先. 2006. 融合 SAR 和 TM 图像更新 GIS 道路网络数据. 测绘学报, **35**(1): 46—51

袁修孝，宋妍. 2007. 一种运用纹理和光谱特征消除投影差影响的建筑物变化检测方法. 武汉大学学报. 信息科学版，**32**(6): 489—493

钟家强，王润生. 2005. 基于自适应参数估计的多时相遥感图像变化检测. 测绘学报, **34**(4): 331—336

钟家强，王润生. 2006. 基于线特征的多时相遥感图像变化检测. 国防科技大学学报, **28**(5): 80—83

朱庆，徐胜华，韩李涛. 2007. 基于 D-S 证据理论的彩色航空影像阴影提取方法. 自动化学报, **33**(6): 588—595